DISCRETE AND CONTINUOUS
DYNAMICAL SYSTEMS SERIES B
Volume **26**, Number **1**, January **2021**

doi:10.3934/dcdsb.2020264

pp. **107–120**

DYNAMICS OF A DISCRETE-TIME STOICHIOMETRIC OPTIMAL FORAGING MODEL

Ming Chen

School of Science, Dalian Maritime University
1 Linghai Road, Dalian, Liaoning, 116026, China

Hao Wang*

Department of Mathematical and Statistical Sciences, University of Alberta
Edmonton, Alberta T6G 2G1, Canada

Abstract. In this paper, we discretize and analyze a stoichiometric optimal foraging model where the grazer's feeding effort depends on the producer's nutrient quality. We systematically make comparisons of the dynamical behaviors between the discrete-time model and the continuous-time model to study the robustness of model predictions to time discretization. When the maximum growth rate of producer is low, both model types admit similar dynamics including bistability and deterministic extinction of the grazer caused by low nutrient quality of the producer. Especially, the grazer is benefited from optimal foraging similarly in both discrete-time and continuous-time models. When the maximum growth rate of producer is high, dynamics of the discrete-time model are more complex including chaos. A phenomenal observation is that under extremely high light intensities, the grazer in the continuous-time model tends to perish due to poor food quality, however, the grazer in the discrete-time model persists in regular or irregular oscillatory ways. This significant difference indicates the necessity of studying discrete-time models which naturally include species' generations and are thus more popular in theoretical biology. Finally, we discuss how the shape of the quality-based feeding function regulates the beneficial or restraint effect of optimal foraging on the grazer population.

1. **Introduction.** Ecological stoichiometry is the study of the balance of energy and essential chemical elements throughout ecological systems [18]. Due to the existence of the chemical heterogeneity between grazers and their food resources, the stoichiometric ratios of elements, such as carbon (C) and phosphorus (P), admit rich dynamics as they vary within and across trophic levels. Loladze et al [10] studied a concise two-dimensional model with Lotka-Volterra type (LKE model) that incorporates stoichiometry into the transfer rate of elements between producer and grazer. This work emphasizes that food quality of producer can cause significant influence on the growth of grazer. LKE model lays a foundation for studying the impact of food quality (P:C) on ecological dynamical model. The main assumption, nutrient is either in the producer or in the grazer, was relaxed in WKL model [20]

2020 *Mathematics Subject Classification.* Primary: 92D25, 92D40; Secondary: 34C05, 34D20.
Key words and phrases. Stoichiometry; food quality; optimal foraging; discrete-time model.
Partially supported by NSFC-11801052, NSFLP-2019-ZD-1056, NSERC RGPIN-2020-03911 and NSERC RGPAS-2020-00090.

* Corresponding Author (hao8@ualberta.ca).

which mechanistically modeled the free nutrient in media. The widely used "strict homeostasis" assumption (also applied in LKE model) was relaxed and carefully examined for its validity in stoichiometric models [22, 23] with one key conclusion that the "strict homeostasis" assumption works for many herbivores except for herbivores with small mortality rates. Based on LKE and WKL models, stoichiometric modeling has been studied from different perspectives [9, 11, 12, 13, 14, 21].

It is generally known that the selection of time scale plays an important role in the study of biology and ecology [6]. The above-mentioned stoichiometric models are continuous in time. Recent studies focused on the robustness of stoichiometric effects to time discretization because discrete-time models naturally include generations of species and are preferred in theoretical biology. Lots of theoretical and numerical comparisons have been done to investigate the departure of dynamical behaviors between continuous-time models and discrete-time models [2, 3, 5, 19, 24]. The existing results show that continuous-time models and their discrete analogues share many similarities. However, populations are more likely to oscillate in discrete-time models.

Optimal foraging theory employs models that aim to predict animal behaviors that maximize their fitness [16]. Many evidences show that foraging strategies employed by herbivores are related to the nutritional contents of their food [8, 17]. Peace and Wang [15] proposed a continuous-time optimal foraging model incorporating the P:C ratio–dependent feeding effort to study the compensatory foraging. Since biologists collect experimental data in discrete time and most species have non-overlapping generations, we develop the discrete-time version of the optimal foraging model to study the robustness and departure of results from the continuous-time model.

The main purpose of this paper is to compare the dynamics of the continuous-time stoichiometric optimal foraging model [15] with its discrete-time analog. We study the discrete-time model in two cases: low and high growth rates of producer. We explore the robustness of some important phenomena exhibited in the continuous-time model by comparing to the discrete-time model, such as bistability, optimal foraging behavior and extinction of grazer caused by low food quality. Furthermore, we explore new dynamical behaviors including chaos in the discrete-time model.

In section 2, we follow the approach developed in [1, 4] to describe the construction of the discrete-time analogue of the stoichiometric optimal foraging model. In section 3, we theoretically study dynamics of the discrete-time model. Section 4 is devoted to investigate the similarities and differences of dynamic behaviors between the discrete-time model and the continuous-time model under low and high growth rates of producer, respectively. Section 5 concludes and discusses our results.

2. **The discrete-time analogue.**

Using stoichiometric principles, Peace and Wang [15] proposed a stoichiometric producer-grazer model with compensatory foraging. The feeding effort defined in [15] is quadratic, which is an unbounded function. To guarantee the extension of solutions in the discrete-time model, we assume that the feeding function admits an upper bound described by a minimum function, which seems scientifically reasonable. Of course, with realistic parameters the results are similar in the absence or presence of this upper bound. The continuous-time optimal foraging model is described by

$$\begin{aligned}\frac{dx}{dt} &= b\min\left\{1-\frac{x}{K},1-\frac{q}{Q}\right\}x-\frac{\mu\xi(Q)x}{1+\mu\xi(Q)\tau x}y,\\ \frac{dy}{dt} &= e\min\left\{1,\frac{Q}{\theta}\right\}\frac{\mu\xi(Q)x}{1+\mu\xi(Q)\tau x}y-\xi(Q)y-\delta\ y,\end{aligned} \tag{1}$$

where

$$Q=\frac{P_T-\theta y}{x} \text{ and } \xi(Q)=\min\{a_0,a_1Q^2+a_2Q+a_3\}.$$

In system (1), $x(t)$ and $y(t)$ represent the densities of producer and grazer (mg C/L), respectively. b denotes the maximum growth rate of producer (day^{-1}). δ is the specific loss rate of grazer including death and respiration (day^{-1}). e is maximum production efficiency in carbon terms for grazer (no unit). It is satisfied that $e<1$ due to the second law of thermodynamics. K is the producer's constant carrying capacity determined by light intensity.

Similar to many stoichiometric models, three assumptions are proposed as follows:

A1: *The total mass of phosphorus in the entire system is fixed, i.e., the system is closed for phosphorus with a total of* P_T (mgP/L).

A2: P : C ratio *in the producer varies, but never falls below a minimum* q (mgP/mgC); *the grazer maintains a constant* P : C, θ (mg P/mg C).

A3: *All phosphorus in the system is divided into two pools:* P *in the grazer and* P *in the producer.*

These assumptions explain the implications of Q and the two minimum functions of system (1). Here, Q describes the variable P quota of the producer. The first minimum function $\min\{1-x/K,1-q/Q\}$ describes the growth rate limited by C (light) and P (nutrient) availability. The second minimum function $\min\{1,Q/\theta\}$ describes the biomass growth rate of grazer, constrained by energy and nutrient limitations.

Considering the compensatory foraging effect, the ingestion rate of grazer (day^{-1}) takes Holling type-II functional response

$$f(x):=\frac{\mu\xi(Q)x}{1+\mu\xi(Q)\tau x},$$

which is called "optimal foraging functional response" [15]. τ represents the handling time, and μ represents the amount of water cleared per mgC invested to generate energy for filtering behavior, $\xi(Q)$ is the feeding effort which is related to the variable P quota of producer Q. Based on [15], $\xi(Q)$ can be described as the quadratic function with an upper bound (a_0) as defined in system (1). The upper and lower bounds of $\xi(Q)$ can be easily found. We denote

$$\breve{\xi}=\min\xi(Q)=\xi(-\frac{a_2}{2a_1})>0 \text{ and } \hat{\xi}=\max\xi(Q)=a_0>0.$$

The above stoichiometric optimal foraging model (1) in continuous time scale can be converted to discrete-time analogue through the method developed in [1, 4]. Considering the differential equations with piecewise constant arguments, we assume that the per capita growth rate stays constant in a given time interval $[t,t+1]$.

TABLE 1. Parameters of model (4) with default values and units

Par.	Description	Value	Unit
P_T	Total phosphorus	0.02	mgPL^{-1}
K	Producer carrying capacity determined by light	$0-3.5$	mgCL^{-1}
b	Maximal growth rate of the producer	1.2 or 3	day^{-1}
δ	Grazer loss rate	0.12	day^{-1}
θ	Grazer constant P : C	0.03	mgP/mgC
q	Producer minimal P : C	0.0038	mgP/mgC
e	Maximal production efficiency in carbon terms for grazer	0.8	
α	Phosphorus half saturation constant of the producer	0.008	mgCL^{-1}
μ	Water cleared/mg C invested to generate filtering energy	700	L/mgC
τ	Handling time (-inverse of max feeding rate)	1.23	day
$\xi(Q)$	Feeding cost, function for optimal foraging model	$a_0 = 0.01, a_1 = 5.17$	
	$\xi(Q) = \min\{a_0, a_1Q^2 + a_2Q + a_3\}$	$a_2 = -0.31, a_3 = 0.007$	

Assume that the per capita growth rates in (1) change only at $t = 0, 1, 2, ...$, then

$$\begin{aligned}
\frac{1}{x(t)}\frac{dx(t)}{dt} &= b\min\left\{1-\frac{x[t]}{K}, 1-\frac{q}{Q}\right\} - \frac{\mu\xi(Q)}{1+\mu\xi(Q)\tau x[t]}y[t],\\
\frac{1}{y(t)}\frac{dy(t)}{dt} &= e\min\left\{1, \frac{Q}{\theta}\right\}\frac{\mu\xi(Q)x[t]}{1+\mu\xi(Q)\tau x[t]} - \xi(Q) - \delta\ , t \neq 0, 1, 2, ...,
\end{aligned} \tag{2}$$

where

$$Q = \frac{P_T - \theta y[t]}{x[t]} \text{ and } \xi(Q) = \min\{a_0, a_1Q^2 + a_2Q + a_3\}.$$

Here $[t]$ represents the integer part of $t \in (0, +\infty)$. We can integrate system (2) on any interval $[n, n+1), n = 0, 1, 2, \cdots$. Then we obtain the following equations for $n \le t < n+1$:

$$\begin{aligned}
x(t) &= x(n)\exp\left\{\left[b\min\left\{1-\frac{x(n)}{K}, 1-\frac{q}{Q}\right\} - \frac{\mu\xi(Q)}{1+\mu\xi(Q)\tau x(n)}y(n)\right](t-n)\right\},\\
y(t) &= y(n)\exp\left\{\left[e\min\left\{1, \tfrac{Q}{\theta}\right\}\frac{\mu\xi(Q)x(n)}{1+\mu\xi(Q)\tau x(n)} - \xi(Q) - \delta\right](t-n)\right\},
\end{aligned} \tag{3}$$

where

$$Q = \frac{P_T - \theta y(n)}{x(n)} \text{ and } \xi(Q) = \min\{a_0, a_1Q^2 + a_2Q + a_3\}.$$

Let $t \to n+1$. Then, the discrete-time analogue of system (1) is well proposed as follows:

$$\begin{aligned}
x(n+1) &= x(n)\exp\left\{b\min\left\{1-\frac{x(n)}{K}, 1-\frac{q}{Q}\right\} - \frac{\mu\xi(Q)}{1+\mu\xi(Q)\tau x(n)}y(n)\right\},\\
y(n+1) &= y(n)\exp\left\{e\min\left\{1, \tfrac{Q}{\theta}\right\}\frac{\mu\xi(Q)x(n)}{1+\mu\xi(Q)\tau x(n)} - \xi(Q) - \delta\right\},
\end{aligned} \tag{4}$$

where

$$Q = \frac{P_T - \theta y(n)}{x(n)} \text{ and } \xi(Q) = \min\{a_0, a_1Q^2 + a_2Q + a_3\}.$$

3. **Model analysis.** In this section, we establish the boundedness and positive invariance for system (4). Then, we analyze the stability of equilibria in system (4).

3.1. **Boundedness and invariance.** In this subsection, we view $f(x)$ as a function of two variables, $f(x,\xi)$. Then we have

$$\frac{\partial f}{\partial x} > 0, \ \frac{\partial f}{\partial \xi} > 0 \quad \text{for } x > 0.$$

For convenience we assume that $f(x,\xi) = xp(x,\xi)$. It is easy to verify that

$$\frac{\partial p}{\partial x} < 0, \ \frac{\partial p}{\partial \xi} > 0 \quad \text{for } x > 0.$$

Theorem 3.1. *For system (4), we have for all $n \in \mathbb{N}^+$,*

$$x(n) \le \max\left\{x(0), \frac{K}{b}\exp(b-1)\right\} \equiv U, \ y(n) \le \max\{y(0), v\}\exp(2\hat{e}f(U,\hat{\xi}) - 2d) \equiv V,$$

where v satisfies $ef\left(U\exp(b - p(U,\breve{\xi})v)\right) < \breve{\xi} + \delta$.

Proof. We can verify that $\max_{x\in\mathbb{R}} x\exp(b - \frac{bx}{K}) = \frac{K}{b}\exp(b-1)$ for $b > 0$. Hence, from system (4) we have

$$x(n+1) < x(n)\exp\left\{b - \frac{bx(n)}{K}\right\} \le \frac{K}{b}\exp(b-1) \equiv u.$$

Then, for all $n \in \mathbb{N}$, we obtain

$$x(n) \le \max\{x(0), u\} \equiv U.$$

If $ef(U,\hat{\xi}) \le \delta$, then we have $y(n) \le y(0)$, for all $n \in \mathbb{N}^+$. Assume below that $ef(U,\hat{\xi}) > \delta$. Let v be large enough that

$$ef\left(U\exp(b - p(U,\breve{\xi})v), \hat{\xi}\right) < \breve{\xi} + \delta.$$

For all $n \in \mathbb{N}$, we obtain

$$y(n) \le \max\{y(0), v\}\exp(2ef(U,\hat{\xi}) - 2\breve{\xi} - 2\delta) \equiv V.$$

This is true for $n = 1, 2$ obviously. We can prove the claim below in two cases.

Case I. $y(0) \le v$. If the claim is not true, then we have $v < y(n_1 - 2) \le V$, $v < y(n_1 - 1) \le V$ and $y(n_1) > V$, for some $n_1 > 2$. By the assumption that $\partial p/\partial x < 0$, we have

$$x(n_1 - 1) \le x(n_1 - 2)\exp(b - p(x(n_1 - 2), \breve{\xi})y(n_1 - 2)) < U\exp(b - p(U,\breve{\xi})v),$$

which implies that

$$y(n_1) < y(n_1 - 1)\exp\{ef[U\exp(b - p(U,\breve{\xi})v), \hat{\xi}] - \breve{\xi} - \delta\} < y(n_1 - 1) \le V.$$

There exists contradiction with $y(n_1) > V$.

Case II. $y(0) > v$. Hence, we obtain $x(1) < U\exp(b - p(U,\breve{\xi})v)$. This implies that $y(2) < y(1)$. In other words, as long as $y(n) > v$, we have $y(n+2) < y(n+1)$. There can be two possibilities: (a) $y(n^*) \le v$ for some $n^* \in \mathbb{N}^+$; (b) $y(n) > v$ for all $n \in \mathbb{N}^+$. In case (a), from the proof of case I, we see that for $y(n) < V$ for $n > n^*$ and hence the claim is also true. In case (b), $y(n)$ is strictly decreasing for $n > 1$ and the claim is true, proving the theorem. □

The above theorem implies the forward invariant set

$$\Delta = \left\{(x,y) : \ 0 < x < \frac{K}{b}\exp(b-1), \ 0 < y < v\right\}.$$

Theorem 3.2. *For system (4), Δ is globally attractive with respect to initial values $(x(0),y(0))$ such that $x(0) > 0$ and $P_T/\theta > y(0) > 0$.*

Proof. From Theorem 3.1, we find that Δ is a positively invariant domain of system (4) and $x(n) \in \big(0, \frac{K}{b}\exp(b-1)\big)$, for large values of n. If $y(n) > v$ for large values of $n \in \mathbb{N}^+$, then $y(n)$ satisfies $y^* = \limsup_{x\to\infty} y(n) \geq v$ due to boundedness. Then, for large values of n, we have

$$y(n) < y(n-1)\exp\{\hat{e}f[U\exp(b - p(U,\breve{\xi})v), \hat{\xi}] - \breve{\xi} - \delta\}.$$

Let $n \to \infty$, we obtain

$$y^* \leq y^*\exp\{\hat{e}f[U\exp(b - p(U,\breve{\xi})v), \hat{\xi}] - \breve{\xi} - \delta\} < y^*,$$

which contradicts $y^* > v > 0$. Thus, we have $y(n) \in (0, v)$, for large values of n. This completes the proof. □

3.2. **Boundary equilibria.** For convenience, we rewrite system (4) as

$$x(n+1) = x(n)\exp\{F(x(n), y(n))\},$$

$$y(n+1) = y(n)\exp\{G(x(n), y(n))\},$$

where

$$F(x,y) = b\min\left\{1 - \frac{x}{K}, 1 - \frac{q}{Q}\right\} - \frac{\mu\xi(Q)}{1+\mu\xi(Q)\tau x}y,$$
$$G(x,y) = e\min\left\{1, \frac{Q}{\theta}\right\}\frac{\mu\xi(Q)x}{1+\mu\xi(Q)\tau x} - \xi(Q) - \delta.$$

Possible equilibrium points of the system (4) can be solved from the equations

$$x[1 - \exp\{F(x,y)\}] = 0, \qquad y[1 - \exp\{G(x,y)\}] = 0.$$

The boundary equilibrium points are $E_0 = (0,0)$ and $E_1 = (k,0)$, where $k = \min\{K, P_T/q\}$

We investigate the stability of equilibria in system (4) by using Jury Test.

Lemma 3.3. *(Jury Test) Let A be a 2×2 constant matrix. Both characteristic roots of A have magnitude less than one if and only if*

$$2 > 1 + Det(A) > |Tr(A)|. \tag{5}$$

The Jacobian of (4) is

$$J(x,y) = \begin{pmatrix} \exp\{F(x,y)\} + x\exp\{F(x,y)\}\dfrac{\partial F(x,y)}{\partial x} & x\exp\{F(x,y)\}\dfrac{\partial F(x,y)}{\partial y} \\ y\exp\{G(x,y)\}\dfrac{\partial G(x,y)}{\partial x} & \exp\{G(x,y)\} + y\exp\{G(x,y)\}\dfrac{\partial G(x,y)}{\partial y} \end{pmatrix}.$$

The stability of boundary equilibria can be described by the following theorem using Jury Test in Lemma 3.3.

Theorem 3.4. *For system (4), E_0 is always unstable. E_1 is locally asymptotically stable (LAS) if*

$$0 < b < 2 \text{ and } e\min\left\{1, \frac{P_T}{k\theta}\right\}\frac{\mu\xi(P_T/k)k}{1+\mu\xi(P_T/k)\tau k} - \xi(P_T/k) - \delta < 0;$$

it is unstable if

$$b > 2 \text{ or } e\min\left\{1, \frac{P_T}{k\theta}\right\}\frac{\mu\xi(P_T/k)k}{1+\mu\xi(P_T/k)\tau k} - \xi(P_T/k) - \delta > 0.$$

Proof. The Jacobian matrix at the origin E_0 becomes

$$J(E_0) = \begin{pmatrix} e^b & 0 \\ 0 & e^{-d} \end{pmatrix}.$$

There exists one characteristic root with magnitude of e^b larger than one. Hence, E_0 is always unstable.

The Jacobian matrix at E_1 turns out to be

$$J(E_1) = \begin{pmatrix} 1-b & k\dfrac{\partial F(x,y)}{\partial y}|_{(k,0)} \\ 0 & \exp\{G(k,0)\} \end{pmatrix},$$

where

$$G(k,0) = e\min\left\{1, \frac{P_T}{k\theta}\right\}\frac{\mu\xi(P_T/k)k}{1+\mu\xi(P_T/k)\tau k} - \xi(P_T/k) - \delta.$$

On one hand, the condition

$$0 < b < 2 \text{ and } e\min\left\{1, \frac{P_T}{k\theta}\right\}\frac{\mu\xi(P_T/k)k}{1+\mu\xi(P_T/k)\tau k} - \xi(P_T/k) - \delta < 0$$

implies that the characteristic roots of $J(E_1)$ are both less than one. Thus E_1 is LAS. On the other hand, E_1 is unstable if one of the opposite strict inequalities holds. □

3.3. **Internal equilibria.**

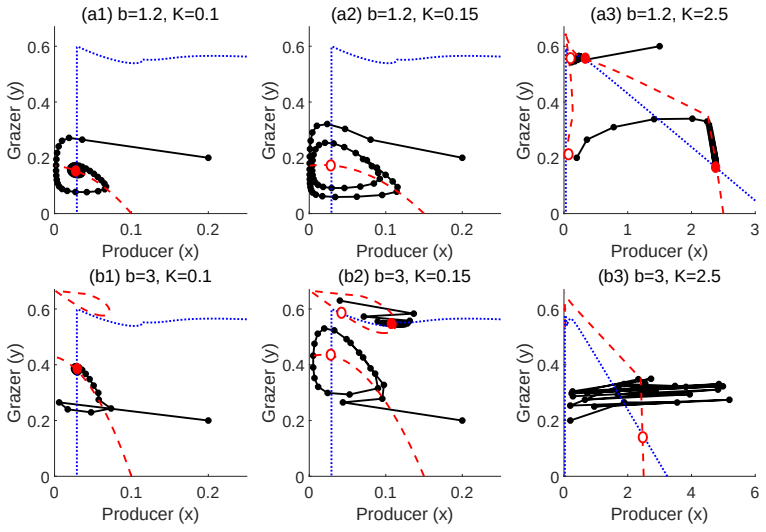

FIGURE 1. Attractor of discrete-time optimal foraging model (4) in phase plane for different light intensities in two cases. Panels of (a_i) describe the case when the producer's growth rate is low $b = 1.2$, $i = 1, 2, 3$. Panels of (b_i) describe the case when the producer's growth rate is high $b = 3$, $i = 1, 2, 3$. The red dashed curves are defined by $F(x, y) = 0$, which denote the producer nullclines. The blue dotted curves are defined by $G(x, y) = 0$, which denote the grazer nullclines. Solid bullets denote stable equilibria while circles represent unstable equilibria.

The internal equilibrium can be found at the interaction of the two nullclines $F(x, y) = 0$ and $G(x, y) = 0$. We discuss the stability of internal equilibria in two cases: Case I, the maximum growth rate of producer is low ($b = 1.2$); Case II, the maximum growth rate of producer is high ($b = 3$). Fig. 1 illustrates the phase portraits of system (4) in two cases as K increases. When the light intensity is very low ($K = 0.1$), the internal equilibrium is stable for both two cases (Fig. 1 (a_1) and (b_1)). When the light intensity increases to intermediate level ($K = 0.15$), there will be a periodic orbit circling around an unstable internal equilibrium (Fig. 1 (a_2) and (b_2)). Specially, there exist multiple internal equilibria in Case II (Fig. 1 (b_2)). Phase trajectory generated from another initial value tends to a stable equilibrium, which shows that system (4) is bistable. When the light intensity further increases to high level ($K = 2.5$), there exist multiple stable equilibria in Case I. (Fig. 1 (a_3)). However, the internal equilibrium is unstable in Case II. The phase trajectory irregularly oscillates and then tends to a singular orbit (Fig. 1 (b_3)).

In general, the internal attractors of system (4) can be either equilibria or a limit cycle when the growth rate of producer is low. However, when the growth rate of producer is high, the attractors can be a singular orbit besides equilibria and a limit cycle. In addition, the discrete-time optimal foraging model exhibits bistability, which means that solution curves with different initial values tend to either one of the two different asymptotic states, such as Fig. 1 (a_3) and (b_2).

4. **Numerical simulations.**

In this section, we will numerically compare dynamical behaviors of the discrete-time model (4) and the continuous-time model (1). We choose the parameter K as the bifurcation parameter, which represents the light intensity. We will discuss the robustness of discretization at low ($b = 1.2$) and high ($b = 3$) maximum growth rates of producer, respectively. The parameters are selected from Table 1 and the initial conditions are set as $x(0) = 0.2$ mg C/L and $y(0) = 0.2$ mg C/L.

4.1. **Low growth rate of producer.**

We first conduct simulations when the producer's growth rate is low ($b = 1.2$). The bifurcation diagrams in Fig. 2 illustrate the transitions of dynamic behaviors in models (4) and (1) as K varies. Fig. 3 presents the solution curves of the two systems, which can be intuitively served as the typical examples with varying K.

For K less than 0.03 mg C/L, the grazer cannot survive due to low food quantity. Fig. 3 (a_1) and (b_1) show such a typical case with $K = 0.02$. When K increases, the grazer can persist at a stable positive equilibrium, and its density increases. A typical example with $K = 0.1$ is shown in Fig. 3 (a_2) and (b_2). When K further increases, the system undergoes a Hopf bifurcation and the equilibrium loses its stability to a limit cycle, whose the amplitude increases as K increases. In the parameter region of a stable limit cycle, there is a subtle difference between discrete-time and continuous-time models. The amplitude of oscillations in the continuous-time model is smaller than that in the discrete-time model (Fig. 3 (a_3) and (b_3)). When K even further increases, the limit cycle disappears through a saddle-node bifurcation and populations return to a new stable equilibrium, as shown in Fig. 3 (a_4) and (b_4). After the saddle-node bifurcation point, the grazer in both continuous-time model (1) and discrete-time model (4) are benefited by optimal foraging, where the grazer remains at a high density (see shaded regions in Fig. 2 (a_2) and (b_2)). When K is sufficiently large, the optimal foraging behavior is

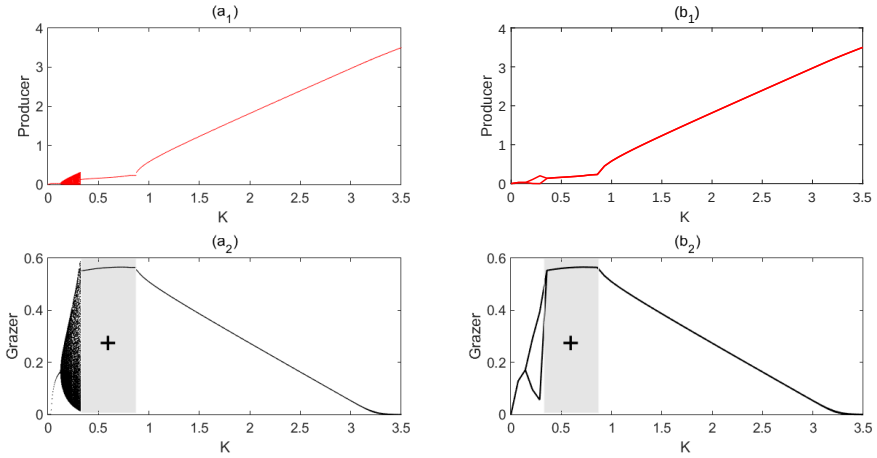

FIGURE 2. Bifurcation diagram of the population densities with respect to K (light intensity) for the discrete-time model (4) (a_i), i=1,2, and the continuous-time model (1) (b_i), i=1,2. Shaded regions with + represent the parameter regions of the optimal foraging behaviors benefiting the grazers. All parameters are provided in Table 1 with $b = 1.2$.

no longer in force. As the grazer's growth is constrained by the gradual worsening food quality, the grazer's density in either model begins to decline and tends to perish. Due to the loss of predation, the producer's density in either model reaches its carrying capacity. Solution curves show this phenomenon in Fig. 3 (a_5) and (b_5).

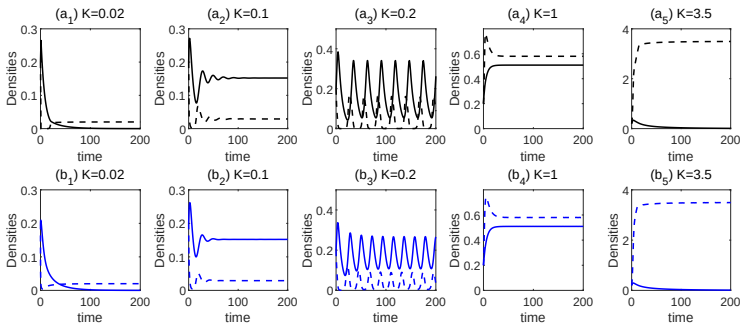

FIGURE 3. Solution curves for system (4) and (1). (a_i) and (b_i) denote the dynamics of (4) and (1) with increasing K, respectively. Producer and grazer's densities (mg C/L) are plotted by dashed and solid lines, respectively. All parameters are provided in Table 1 with $b = 1.2$.

4.2. **High growth rate of producer.** In fact, discretization can cause significant differences on the dynamics of system (1) when the maximum growth rate of producer is high ($b = 3$). Some parameter sets yield different dynamics for models (4) and (1). When $K = 0.15$, populations of the continuous-time model tend to a positive stable equilibrium, while those of the discrete-time model show periodic

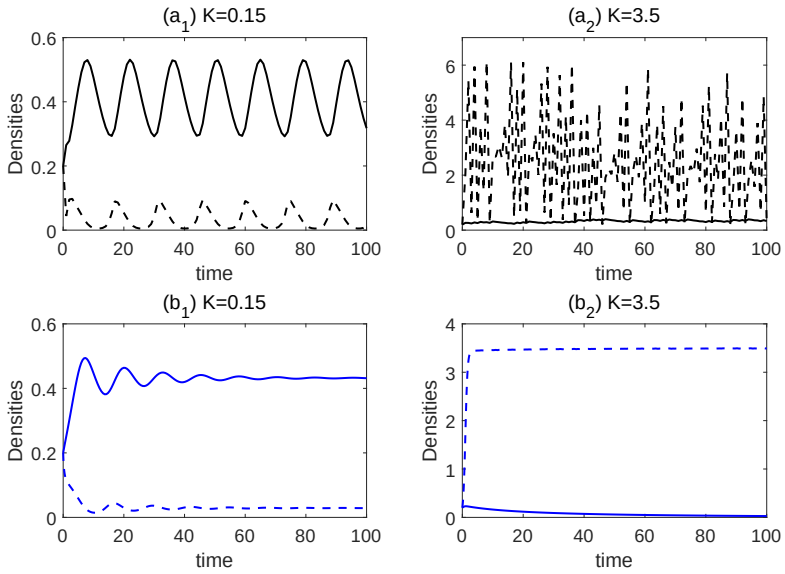

FIGURE 4. Solution curves for system (4) and (1). (a_i) and (b_i) denote the dynamics of (4) and (1) with increasing K, respectively. Producer and grazer densities (mg C/L) are described by dashed and solid lines, respectively. All parameters are provided in Table 1 with $b = 3$.

oscillations (Fig. 4 (a_1) and (b_1)). When $K = 3.5$, populations of the continuous-time model tend to a boundary stable equilibrium, while those of the discrete-time model show chaotic behaviors (Fig. 4 (a_2) and (b_2)).

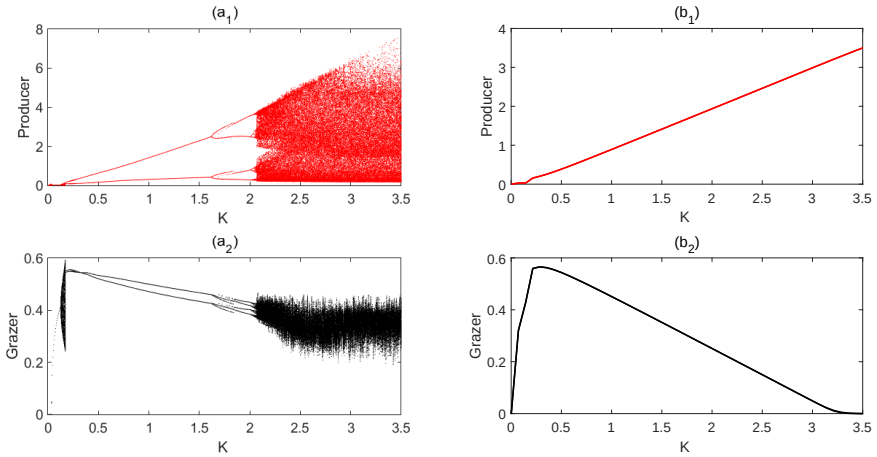

FIGURE 5. The bifurcation curves with respect to K for the discrete-time model (a_i), i=1,2, and continuous-time model (b_i), i=1,2. All parameters are provided in Table 1 with $b = 3$.

Bifurcation diagrams with the high growth rate of producer are sketched in Fig. 5. Different from the case with the low growth rate of producer, we cannot observe

obvious optimal foraging behavior when the growth rate of producer is high. One can observe that dynamics of the continuous-time model (1) and the corresponding discrete-time model (4) are completely different as exhibited in Fig. 5. The species in the discrete-time model can coexist and the system is persistent even when the light intensity is extremely high (Fig. 5 (a_1) and (a_2)). However, Fig. 5 (b_2) shows the extinction of grazer in the continuous-time model under extremely high light intensities.

Additionally, the attractor in continuous-time model (1) can be the boundary equilibrium or the internal equilibrium (Fig. 5 (b_1) and (b_2)). However, in discrete-time model (4), besides boundary equilibrium and internal equilibrium, the attractor can also be a limit cycle or even a strange attractor (chaos) as shown in Fig. 5 (a_1) and (a_2). In Fig. 6, when K varies within the intervals $(0.01, 0.05)$ and $(2.1, 3.5)$, the maximum Lyapunov exponent (MLE) of system (4) is positive, which proves that the discrete-time model indeed has chaos. Fig. 5 (a_1) and (a_2) show the pathway from period-doubling to chaos. Hence, discretization can lead to regular and irregular oscillations of populations.

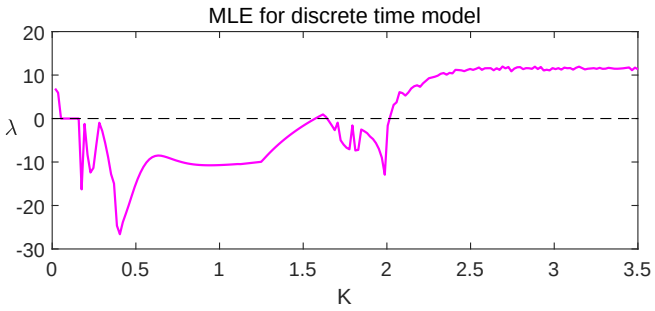

FIGURE 6. Spectrum of the maximum Lyapunov exponent (MLE) with respect to K for the discrete-time model. All parameters are provided in Table 1 with $b = 3$.

5. **Discussion.** In this paper, we discretized the optimal foraging model in [15] by applying the method developed in [1, 4]. Different from most other stoichiometric models, the grazer ingestion rate is considered as a Holling type II functional response that depends not only on the producer's quantity but also on its quality. We rigorously investigated the asymptotic stability of equilibria in the discrete-time model. We explored the dynamical behaviors of the discrete-time model through numerical solutions and bifurcation diagrams and compared them with the continuous-time model.

When the maximum growth rate of producer is low, the results of the continuous-time model are robust to time discretization. Most important dynamical features exhibited in the continuous-time optimal foraging model can also be observed in the discrete-time model, such as bistability, optimal foraging behavior and deterministic extinction of grazer due to poor food quality.

When the growth rate of producer is high, one can observe significant differences in dynamical behaviors between discrete-time and continuous-time models. When faced with extremely high light intensities, the grazer in the continuous-time model tends to perish due to poor food quality. However, the dynamical behaviors of the discrete-time model show that the grazer can coexist with the producer under

extremely strong light. Furthermore, populations in the continuous-time model tend to a steady state, while the discrete-time model shows richer dynamics, such as periodic oscillations or even chaos.

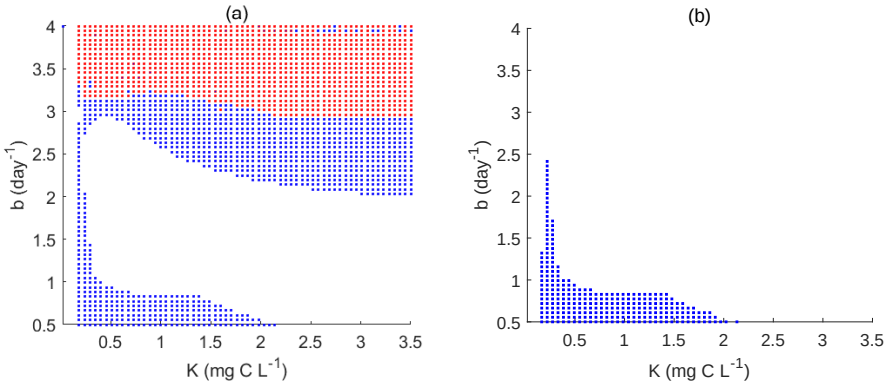

FIGURE 7. A two-parameter bifurcation diagram for varying light level K and varying maximal growth rate of producer b for the discrete-time model (a) and continuous-time model (b). All other parameter values are listed in Table 1 and the initial point is $x(0) = 0.2$ mgCL^{-1} and $y(0) = 0.2$ mgCL^{-1}. Discrete-time model (4) exhibits periodic oscillations in blue region and chaotic behaviors in red region. Outside these regions, model (4) has stable equilibria.

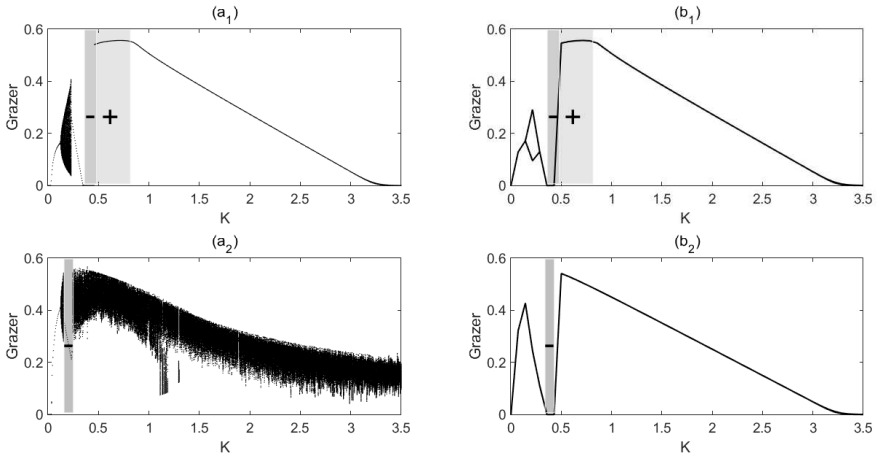

FIGURE 8. Bifurcation diagram of the grazer densities with respect to K (light intensity) for the discrete-time model (4) (a_i), i=1,2, and the continuous-time model (1) (b_i), i=1,2. Specially, (a_1) and (b_1) denote the case with the low growth rate of producer ($b = 1.2$); (a_2) and (b_2) denote the case with the high growth rate of producer ($b = 3$). Light (+) and dark (−) shaded regions represent the parameter regions of the optimal foraging behaviors benefiting and restraining the grazers, respectively. All parameters are provided in Table 1 except the parameter $a_1 = 3.5$.

We classify the behaviors of discrete-time model (4) and continuous-time model (1) in b-K planes (Fig. 7). For discrete-time model (4), the red region of Fig. 7(a) shows that chaotic behavior occurs when the growth rate is high and the light

intensity is not too low. The attractor can also be a limit cycle (the blue region) or a steady state (the white region). Comparing (a) and (b) of Fig. 7, we find that the parameter region driving oscillations for discrete-time model is far larger than that for continuous-time model.

The shape of the optimal foraging function $\xi(Q)$ can greatly affect the grazer dynamics. In the optimal foraging function, a_1 is a key parameter governing the width of "open mouth" of the quality-dependent feeding effort. We decrease $a_1 = 5.17$ in Table 1 to $a_1 = 3.5$ in Fig. 8. Compared with Fig. 2 (a_2) and (b_2), we can observe that the grazer can be either benefited from optimal foraging in the light grey region with + or constrained by optimal foraging in the dark grey region with − in Fig. 8 (a_1) and (b_1). Compared with Fig. 5 (a_2) and (b_2) with no obvious optimal foraging behaviors, the grazer is inhibited by optimal foraging in Fig. 8 (a_2) and (b_2). The inhibition effect occurs at lower light intensities in the discrete-time model than in the continuous-time model. Lower a_1 in the quality-based feeding function leads to the purely negative impact of optimal foraging on the grazer population.

REFERENCES

[1] S. Busenberg and K. L. Cooke, Models of vertically transmitted diseases with sequential-continuous dynamics, *Nonlinear Phenomena in Mathematical Sciences*, (1982), 179–187.

[2] M. Chen, M. Fan, C. B. Xie, A. Peace and H. Wang, Stoichiometric food chain model on discrete time scale, *Mathematical Biosciences and Engineering*, **16** (2018), 101–118.

[3] M. Chen, L. Asik and A. Peace, Stoichiometric knife-edge model on discrete time scale, *Advances in Difference Equations*, **2019** (2019), 1–16.

[4] K. L. Cooke and J. Wiener, Retarded differential equations with piecewise constant delays, *Journal of Mathematical Analysis and Applications*, **99** (1984), 265–297.

[5] M. Fan, I. Loladze, Y. Kuang and J. J. Elser, Dynamics of a stoichiometric discrete producer-grazer model, *Journal of Difference Equations and Applications*, **11** (2005), 347–364.

[6] R. Frankham and B. W. Brook, The importance of time scale in conservation biology and ecology, *Annales Zoologici Fennici*, **41** (2004), 459–463.

[7] W. Gurney and R. M. Nisbet, *Ecological Dynamics*, 1998.

[8] J. J. Elser, M. Kyle, J. Learned, M. McCrackin, A. Peace and L. Steger, Life on the stoichiometric knife-edge: Effects of high and low food C:P ratio on growth, feeding, and respiration in three Daphnia species, *Inland Waters*, **6** (2016), 136–146.

[9] Y. Kuang, J. Huisman and J. J. Elser, Stoichiometric plant-herbivore models and their interpretation, *Mathematical Biosciences and Engineering*, **1** (2004), 215–222.

[10] I. Loladze, Y. Kuang and J. J. Elser, Stoichiometry in producer-grazer systems: Linking energy flow with element cycling, *Bulletin of Mathematical Biology*, **62** (2000), 1137–1162.

[11] I. Loladze, Y. Kuang, J. J. Elser and W. F. Fagan, Competition and stoichiometry: Coexistence of two predators on one prey, *Theoretical Population Biology*, **65** (2004), 1–15.

[12] A. Peace, Y. Zhao, I. Loladze, J. J. Elser and Y. Kuang, A stoichiometric producer-grazer model incorporating the effects of excess food-nutrient content on consumer dynamics, *Mathematical Biosciences*, **244** (2013), 107–115.

[13] A. Peace, H. Wang and Y. Kuang, Dynamics of a producer-grazer model incorporating the effects of excess food nutrient content on grazer's growth, *Bulletin of Mathematical Biology*, **76** (2014), 2175–2197.

[14] A. Peace, Effects of light, nutrients, and food chain length on trophic efficiencies in simple stoichiometric aquatic food chain models, *Ecological Modelling*, **312** (2015), 125–135.

[15] A. Peace and H. Wang, Compensatory foraging in stoichiometric producer-grazer models, *Bulletin of Mathematical Biology*, **81** (2019), 4932–4950.

[16] G. H. Pyke, H. R. Pulliam and E. L. Charnov, Optimal Foraging: A selective review of theory and tests, *Quarterly Review of Biology*, **52** (1977), 137–154.

[17] S. J. Simpson, R. M. Sibly, K. P. Lee, S. T. Behmer and D. Raubenheimer, Optimal foraging when regulating intake of multiple nutrients, *Animal Behaviour*, **68** (2004), 1299–1311.

[18] R. W. Sterner and J. J. Elser, *Ecological Stoichiometry: The Biology of Elements from Molecules to the Biosphere*, Princeton University Press, 2002.
[19] G. Sui, M. Fan, I. Loladze and Y. Kuang, The dynamics of a stoichiometric plant-herbivore model and its discrete analog, *Mathematical Biosciences and Engineering*, **4** (2007), 29–46.
[20] H. Wang, Y. Kuang and I. Loladze, Dynamics of a mechanistically derived stoichiometric producer-grazer model, *Journal of Biological Dynamics*, **2** (2008), 286–296.
[21] H. Wang, K. Dunning, J. J. Elser and Y. Kuang, Daphnia species invasion, competitive exclusion, and chaotic coexistence, *Discrete & Continuous Dynamical Systems-B*, **12** (2009), 481–493.
[22] H. Wang, R. W. Sterner and J. J. Elser, On the "strict homeostasis" assumption in ecological stoichiometry, *Ecological Modelling*, **243** (2012), 81–88.
[23] H. Wang, Z. Lu and A. Raghavan, Weak dynamical threshold for the "strict homeostasis" assumption in ecological stoichiometry, *Ecological Modelling*, **384** (2018), 233–240.
[24] C. Xie, M. Fan and W. Zhao, Dynamics of a discrete stoichiometric two predators one prey model, *Journal of Biological Systems*, **18** (2010), 649–667.

Received April 2020; revised June 2020.

E-mail address: chenm688@dlmu.edu.cn
E-mail address: hao8@ualberta.ca